

Performance boost of time-delay reservoir computing by non-resonant clock cycle

Florian Stelzer^{1,2,*}, André Röhm³, Kathy Lüdge³, and Serhiy Yanchuk¹

¹Institute of Mathematics, Technische Universität Berlin

²Department of Mathematics, Humboldt-Universität zu Berlin

³Institute of Theoretical Physics, Technische Universität Berlin

September 2, 2022

*

Abstract

The time-delay-based reservoir computing setup has seen tremendous success in both experiment and simulation. It allows for the construction of large neuromorphic computing systems with only few components. However, until now the interplay of the different timescales has not been investigated thoroughly. In this manuscript, we investigate the effects of a mismatch between the time-delay and the clock cycle for a general model. Typically, these two time scales are considered to be equal. Here we show that the case of equal or rationally related time-delay and clock cycle could be actively detrimental and leads to an increase of the approximation error of the reservoir. In particular, we can show that non-resonant ratios of these time scales have maximal memory capacities. We achieve this by translating the periodically driven delay-dynamical system into an equivalent network. Networks that originate from a system with resonant delay-times and clock cycles fail to utilize all of their degrees of freedom, which causes the degradation of their performance.

keywords: time-delay; reservoir computing; clock cycle; resonance; memory capacity; network representation

*Corresponding author

stelzer@math.tu-berlin.de, aroehm@mailbox.tu-berlin.de, kathy.luedge@tu-berlin.de, yanchuk@math.tu-berlin.de

1 Introduction

Reservoir computing is a machine learning method, which was introduced independently by both Jaeger [1] as a mathematical framework and by Maas et al. [2] from a biologically inspired background. It fundamentally differs from many other machine learning concepts and is particularly interesting due to its easy integration into hardware, especially photonics [3, 4]. With the help of the reservoir computing paradigms, the naturally occurring computational power of almost any dynamical or physical system can be exploited. It is particularly valuable for solving the class of time-dependent problems, which is usually neglected by artificial neural network-based approaches. A time-dependent problem requires to estimate a target signal $(y(t))_{t \in \mathbb{T}}$ which depends non-trivially on an input signal $(u(t))_{t \in \mathbb{T}}$, the set of times \mathbb{T} may be continuous or discrete. This class of problems contains, in particular, speech recognition or time series prediction [5, 6, 7], and also has great promise for error correction in optical data transmission [8]. Furthermore, reservoir computing can be used to study fundamental properties of dynamical systems in a completely novel way [9], enabling new ways of characterizing physical systems.

The main idea of reservoir computing is simple, yet powerful: A dynamical system, the *reservoir*, is driven by an input $u(t)$. The state of the reservoir is described by a variable $x(t)$, which can be high- or even infinite-dimensional. A linear *readout mapping* $x(t) \mapsto \hat{y}(t)$ provides an output. While the parameters of the reservoir itself remain fixed at all times, the coefficients of the linear mapping $x(t) \mapsto \hat{y}(t)$ are subject to adaptation, i.e. the readout can be trained.

Reservoir computing is a supervised machine learning method. An input $u(t)$ and the corresponding target function $y(t)$ are given as a training example. Then optimal output weights, i.e. coefficients of the linear mapping $x(t) \mapsto \hat{y}(t)$, are determined such that $\hat{y}(t)$ approximates the target $y(t)$. This is analogous to a conventional artificial neural network where only the last layer is trained. The goal of this procedure is to approximate the mapping $u(t) \mapsto y(t)$ via $u(t) \mapsto x(t) \mapsto \hat{y}(t)$ such that it not only reproduces the target function for the given training input but also provides meaningful results for other, in certain sense similar, inputs. From a nonlinear dynamics perspective, the readout mapping $x(t) \mapsto \hat{y}(t)$ is a linear combination of different degrees of freedom of the system.

The reservoir must fulfill several criteria to exhibit good computational properties: First, it must be able to carry information of multiple past input states, i.e. have memory. References [10] and [11] study how a reservoir can store information about past inputs. Second, the system should contain a non-linearity to allow for non-trivial data processing. Jaeger [1] proposed to use a recurrent neural network with random connections as reservoir. In this case the reservoir x has a high-dimensional state space by design, as the dimension equals the number of nodes. Such systems are in general able to store a large amount of information. Moreover, the recurrent structure of the network ensures that information about past input states remains for a number of time steps and fades slowly. Jaeger compared the presence of past inputs in the state of x to echoes. For this reason he called his proposed reservoir system *echo state network*.

In recent years, the field of reservoir computing has profited from experimental approaches that use a continuous time-delay dynamical system as reservoir [12]. While hybrid network-delay systems have also been proposed [13], typically, only a single dynamical nonlinear system is employed and connected to a long delay loop; i.e. as opposed to a network-based approach only a single active element is needed for a delay-based reservoir. Here, the complexity is induced by the inherent large phase space dimension of the dynamical system with time-delay [14, 15, 16]. The main advantage of using a delay system over Jaeger’s echo state approach [1] is that one can physically implement the delay system with analogue hardware at relatively low costs—either electronically [12] or even optically [17, 18].

Two main time scales exist in such delay-based reservoir systems: the delay-time τ given by the physical length of the feedback line, and a clock cycle τ' given by the input speed. In this paper, we show that the non-trivial cases of mismatched delay-time and clock cycle possess better reservoir computing properties. We explain this by studying the corresponding equivalent network, where we can show that non-resonant ratios of τ' to τ have maximal memory capacities.

The paper is organized as follows: In section 2 the general model of a reservoir computer based on a single delay-differential system is introduced. We refer to this method as *time-delay reservoir computing* (TDRC). Section 3 shows numerical simulations and the effect of mismatching clock cycles and delay-times. Section 4 derives a representation of the TDRC system with mismatching clock cycle and delay-time as an equivalent echo state network. Section 5 presents a direct calculation of the memory capacity. Section 6 derives a semi-analytic explanation for the observed decreased memory capacity for resonant τ' to τ ratios and provides an intuitive interpretation. All results are summarized in section 7.

2 Time-delay reservoir computing

In this section we describe the reservoir computing system based on a delay equation. Its choice is inspired by the publications [12, 17], where it was experimentally implemented using analogue hardware. In comparison to the general reservoir computing scheme $u(t) \mapsto x(t) \mapsto \hat{y}(t)$ described above, an additional ‘preprocessing’ step is added to transform the input u in an appropriate way before being sent to the reservoir. This is particularly necessary when the input u is discrete and the reservoir x is time-continuous. In the following, we describe the resulting chain of transformations

$$u \xrightarrow{\text{(I)}} J(t) \xrightarrow{\text{(II)}} x(t) \xrightarrow{\text{(III)}} \hat{y}(t) \tag{1}$$

in detail.

2.1 Step (I): preprocessing of the input

Since the reservoir is implemented with the physical experiment in mind (e.g. semiconductor laser), its state variable $x(t)$ is time-continuous. However, the input data is discrete in typical applications of TDRC [12, 13, 17]. For this reason the preprocessing function $u \mapsto J(t)$ translates the discrete input u into a continuous function $J(t)$.

We consider a discrete input sequence $(u(k))_{k \in \mathbb{N}_0}$, where $u(k) \in \mathbb{R}$ is one-dimensional, however, the method can be extended to multi-dimensional inputs. The important parameters that define the preprocessing are the clock cycle $\tau' > 0$, number of virtual nodes $N \in \mathbb{N}$ and the resulting time per virtual node $\theta := \tau'/N$. Previous results [12] suggest the following ranges for the values of these parameters: the clock cycle should be of the order of the delay τ , and the time per virtual node θ of the order of the reservoir timescale.

First, a function $\bar{u}(t)$ is defined as step function

$$\bar{u}(t) := u(k), \quad t \in [k\tau', (k+1)\tau'), \quad k \in \mathbb{N}_0 \quad (2)$$

with step length τ' . Using the indicator function

$$\Pi_M(t) = \begin{cases} 1, & t \in M, \\ 0, & t \notin M, \end{cases} \quad (3)$$

the definition of \bar{u} can be equivalently written as

$$\bar{u}(t) = \sum_{k \in \mathbb{N}_0} u(k) \Pi_{[k\tau', (k+1)\tau')}(t). \quad (4)$$

Secondly, $\bar{u}(t)$ is multiplied by the τ' -periodic mask

$$\mathcal{M}(t) = \sum_{n=1}^N w_n \Pi_{[(n-1)\theta, n\theta)}(t \bmod \tau'), \quad (5)$$

which is piecewise constant with step length $\theta = \tau'/N$ and values w_n . Multiple options for the choice of a mask function are compared in reference [19]. The final preprocessed input signal $J(t)$ is

$$\begin{aligned} J(t) &:= \mathcal{M}(t) \bar{u}(t) \\ &= \sum_{\substack{k \in \mathbb{N}_0 \\ 1 \leq n \leq N}} w_n u(k) \Pi_{[k\tau' + (n-1)\theta, k\tau' + n\theta)}(t). \end{aligned} \quad (6)$$

It is a piecewise constant function with values

$$J_{k,n} := w_n u(k) \quad (7)$$

on the intervals $[k\tau' + (n-1)\theta, k\tau' + n\theta)$. The details of the preprocessing are illustrated in figure 1.

For further analysis, it is convenient to denote the ‘mask’-vector W^{mask} and the input vector J_k as follows:

$$W^{\text{mask}} := (w_1, \dots, w_N)^T, \quad J_k = W^{\text{mask}} u(k). \quad (8)$$

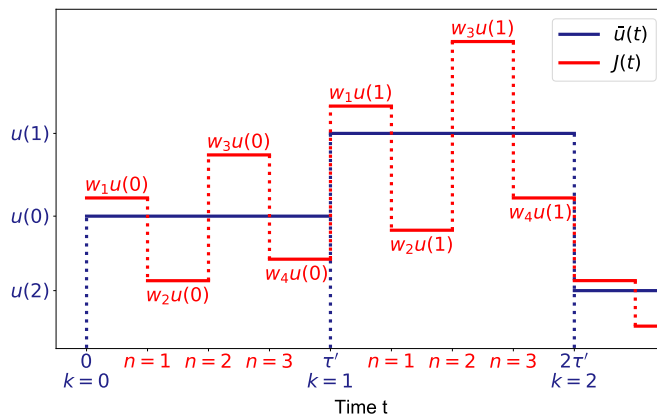


Figure 1: Schematic representation of the preprocessing step: the discrete input sequence $u(0), u(1), \dots$ defines the a function $\bar{u}(t)$ (blue), which is multiplied by a τ' -periodic mask function $\mathcal{M}(t)$ to obtain the preprocessed input $J(t)$ (red). Here the length of the mask vector is $N = 4$. The resulting function $J(t)$ enters the reservoir equation (9).

2.2 Step (II): reservoir

Inspired by the previous works [12], we study the reservoir given by the delay-differential equation

$$\frac{dx}{dt}(t) = -x(t) + f[x(t - \tau) + \gamma J(t)], \quad (9)$$

where $\tau > 0$ is the delay-time, $\gamma > 0$ is the input strength, $f: \mathbb{R} \rightarrow \mathbb{R}$ the activation function, and $J(t)$ the preprocessed input function. The term $-x(t)$ in equation (9) induces the ‘fading memory’ property necessary for the reservoir [1].

For a given preprocessed input $J(t)$, the reservoir variable is computed by solving the delay-differential equation (9) with some initial condition. For a properly chosen reservoir, the initial conditions does not play an important role. This is related to the phenomenon of generalized synchronization [20, 21] but we do not address this question in this work in details. In short, generalized synchronization in reservoir computing means that identical reservoirs which are driven by the same input but have different initial states will approximate each other asymptotically. In the literature about reservoir computing this property is often referred to as *echo state property*.

2.3 Step (III): readout

The continuous reservoir variable $x(t)$ needs to be discretized for the output. For this, the dynamical system is read out every θ time units. Because every

small time window $[k\tau' + (n-1)\theta, k\tau' + n\theta]$ is fed with its own input $J_{k,n}$, these time windows are often seen as ‘virtual nodes’, and the whole delay system as a ‘virtual network’ [12, 22]. We discretize the reservoir variable correspondingly:

$$X(k) := \begin{pmatrix} X_1(k) \\ \vdots \\ X_N(k) \end{pmatrix} := \begin{pmatrix} x((k-1)\tau' + \theta) \\ x((k-1)\tau' + 2\theta) \\ \vdots \\ x((k-1)\tau' + N\theta) \end{pmatrix}. \quad (10)$$

In fact, $X(k)$ is the vector containing the N -point discretization of the variable $x(t)$ on the interval $((k-1)\tau', k\tau']$. The output $\hat{y} = (\hat{y}(k))_{k \in \mathbb{N}_0}$ of the machine learning system is defined as

$$\hat{y}(k) = W^{\text{out}}X(k) + c, \quad (11)$$

where W^{out} is an N -dimensional row vector and $c \in \mathbb{R}$ is a scalar bias. The output weight variables W^{out} and c are to be adjusted in the training process and are chosen by linear regression for reservoir computers [1].

3 Effect of the mismatch between delay and clock cycle times

When TDRC was first introduced, the clock cycle τ' for the preprocessing of the input mask was chosen to be equal to the delay τ [12, 17]. In this case one can easily find an ‘equivalent network’ which is a discrete approximation of the reservoir system. See the supplementary material of [12] or reference [23] for an example. However, recent numerical observations show, that the performance may be improved if one sets $\tau' \neq \tau$. The earliest example of this can be arguably found in reference [24].

We use the NARMA-10 task [25] and the memory capacity (MC) [10] to measure the performance of a simple TDRC to illustrate the role of the clock cycle τ' . These are typical benchmark tasks and we refer to the appendix for a detailed explanation. Let the activation function f in equation (9) be a linear function

$$f(x) = \alpha x. \quad (12)$$

with $\alpha = 0.9$. The other parameters are set to $\tau = 80$, $N = 50$, and $\gamma = 0.02$. We trained this system on 5000 data points for the NARMA-10 task with a regularization by a white noise term with the amplitude 10^{-8} . For our tests we fix an input weight vector W^{mask} with independently $\mathcal{U}(-1, 1)$ -distributed entries w_n . We simulate 100 different masks and train the output weights for each of the mask for 5000 input steps, and then evaluate the learned behavior on an independent set of 2000 samples.

The top panel of figure 2 shows the results of simulations with these parameters. The normalized mean square error (NRMSE, see equation (98)) is

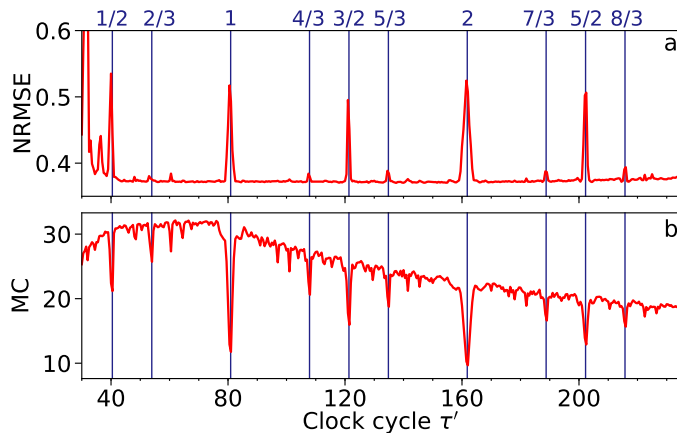


Figure 2: This plot shows the NRMSE of a linear TDRC for the NARMA-10 task (top) and the total memory capacity MC_{tot} (bottom). Clearly visible are error peaks for values of τ' that are close to integer multiples of τ and low-order resonances. Vertical lines denote the resonant values $\tau'/\tau = 1/2, 2/3, 1, 4/3, 3/2, 5/3, 2, 7/3, 5/2, \text{ and } 8/3$. Other parameters are $\alpha = 0.9, \tau = 80, N = 50$, and $\gamma = 0.02$. The reservoir is trained on 5000 samples and evaluated on 2000 samples with a regularization by a noise of $\beta = 10^{-8}$ added to the output of the reservoir. The results are averaged for 100 different random input masks.

a quantitative measure of the systems performance. The error can in general depend on many parameters. Figure 2 shows that the linear network exhibits clear peaks of the error for certain values of the clock cycle τ' . These peaks are located close to low-order resonances with the delay-time $\tau = 80$ and fulfill the relation $a\tau \approx b\tau'$ for small $a, b \in \mathbb{N}$. In fact, the peaks are located slightly above the resonant τ' values. The lower panel of Figure 2 reveals at least part of the reason for this: The total memory capacity for these resonant clock cycles decreases dramatically.

The rest of this paper is devoted to the explanation of this phenomenon. Using a linear activation function is not the optimal choice for the TDRC. However, the resonance effects that we are interested in are general and have been numerically verified to be largely independent of f . They do however get enhanced by a stronger regularization. Conversely, if the system is large enough, i.e. for large N , the effect reduces and can be mostly ignored for simple tasks like NARMA-10.

4 Approximation by a network

In order to explain the degradation of the memory capacity for the resonant clock cycles, we present the delay-system reservoir as an equivalent network. Similar procedure was done in [12] for a TDRC with Mackey-Glass activation function

and $\tau' = \tau$. (See the supplementary material of [12].) However, our case is more complicated, as we allow for $\tau' \neq \tau$. This changes the coupling matrix of the resulting equivalent network. Since a detailed derivation is technical, we move it to Appendix A and present the main results in this section.

As follows from Appendix A, the TDRC dynamics can be approximated by the discrete mapping

$$\begin{aligned} \tilde{X}(k+1) = B\tilde{X}(k) + (1 - e^{-\theta})F \left[A_q\tilde{X}(k+1-\ell) \right. \\ \left. + A_{-(N-q)}\tilde{X}(k-\ell) + \gamma J_k \right], \end{aligned} \quad (13)$$

where

$$\tilde{X}(k) := A_0^{-1}X(k) \quad (14)$$

and $X(k)$ is the discretized vector of the reservoir defined in equation (10). Let us define and explain further notations used in the mapping (13). The matrix

$$A_0 := \begin{pmatrix} 1 & 0 & \dots & 0 \\ e^{-\theta} & 1 & \ddots & \vdots \\ \vdots & \ddots & \ddots & 0 \\ e^{-(N-1)\theta} & \dots & e^{-\theta} & 1 \end{pmatrix} \quad (15)$$

is the classical coupling matrix of an equivalent network for TDRC with $\tau' = \tau$ [12]. Moreover,

$$\begin{aligned} \ell &:= \left\lfloor \frac{m}{N} \right\rfloor, \quad q := m \bmod N, \\ m &:= \left\lceil \frac{\tau}{\theta} \right\rceil = \left\lceil \frac{\tau}{\tau'} N \right\rceil, \quad \theta = \frac{\tau'}{N}, \end{aligned} \quad (16)$$

where $\lfloor \cdot \rfloor$ and $\lceil \cdot \rceil$ denote the floor and the ceiling function, which we need to employ to allow delay-times τ that are not an integer multiple of θ . These quantities can be interpreted as follows: m is the number of virtual nodes that are needed to cover a τ -interval, q is a measure of the misalignment between τ and τ' , and ℓ is roughly the ratio between the delay-time τ and the clock cycle τ' . For $\ell = 0$, the delay τ is shorter than the clock cycle τ' , and it is similar to or larger than the clock cycle for $\ell \geq 1$. The matrices A_q and $A_{-(N-q)}$ are shifted versions of the matrix A_0 . They are defined as follows:

$$A_q := \begin{pmatrix} 0 & \dots & \dots & \dots & \dots & \dots & 0 \\ \vdots & & & & & & \vdots \\ 0 & & & & & & \vdots \\ 1 & 0 & & & & & \vdots \\ e^{-\theta} & 1 & \ddots & & & & \vdots \\ \vdots & \ddots & \ddots & 0 & & & \vdots \\ e^{-(N-1-q)\theta} & \dots & e^{-\theta} & 1 & 0 & \dots & 0 \end{pmatrix} \quad (17)$$

is obtained by a downwards shift of A_0 by q rows and

$$A_{-(N-q)} := \begin{pmatrix} e^{-(N-q)\theta} & \dots & e^{-2\theta} & e^{-\theta} & 1 & 0 & \dots & 0 \\ \vdots & & & \ddots & \ddots & \ddots & \ddots & \vdots \\ \vdots & & & & \ddots & \ddots & \ddots & 0 \\ e^{-(N-1)\theta} & \dots & \dots & \dots & \dots & e^{-2\theta} & e^{-\theta} & 1 \\ 0 & \dots & \dots & \dots & \dots & 0 & 0 & 0 \\ \vdots & & & & & & & \vdots \\ 0 & \dots & \dots & \dots & \dots & \dots & \dots & 0 \end{pmatrix} \quad (18)$$

is obtained by the upwards shift of A_0 by $N - q$ rows. Furthermore

$$B := \begin{pmatrix} e^{-N\theta} & \dots & e^{-\theta} \\ 0 & \dots & 0 \\ \vdots & & \vdots \\ 0 & \dots & 0 \end{pmatrix}, \quad (19)$$

$$F \begin{pmatrix} x_1 \\ \vdots \\ x_N \end{pmatrix} := \begin{pmatrix} f(x_1) \\ \vdots \\ f(x_N) \end{pmatrix}, \quad (20)$$

and J_k is defined as the input vector (8).

The mapping (13) generalizes previous results from [12, 22]. If the clock cycle τ' satisfies $\tau' \in [\tau, \tau + \theta)$, the description coincides with the classical case $\tau' = \tau$ and the approximate equation (13) yields the same mapping

$$\tilde{X}(k+1) = B\tilde{X}(k) + (1 - e^{-\theta})F[A_0\tilde{X}(k) + \gamma J_k] \quad (21)$$

as presented in [12] because then $\ell = 1$, $q = 0$, and $A_{-(N-q)} = 0$.

Analytical approaches for the nonlinear system (13) can be difficult. To simplify, we will study the effect of different clock cycles τ' with the help of a linear activation function $f(x) = \alpha x$, where α is a scalar. Then equation (13) can be written as

$$\begin{aligned} \tilde{X}(k+1) = & B\tilde{X}(k) + \nu\alpha[A_q\tilde{X}(k+1-\ell) \\ & + A_{-(N-q)}\tilde{X}(k-\ell) + \gamma W^{\text{mask}}u(k)] \end{aligned} \quad (22)$$

by plugging in $W^{\text{mask}}u(k)$ for J_k and by writing $\nu := 1 - e^{-\theta}$ for the sake of shortness.

System (13) possesses the following properties: in the case $\tau' \geq \tau + \theta$, we have $\ell = 0$, and hence, equation (13) is in general an implicit map. This is the physical case of a delay shorter than the clock cycle, which means that the feedback from some of the virtual nodes will act on other virtual nodes within

the same cycle. However, for the linear activation function in equation (22) and by (14) we obtain the explicit map

$$X(k+1) = AX(k) + W^{\text{in}}u(k), \quad (23)$$

where

$$A := A_0(\text{Id} - \nu\alpha A_q)^{-1}(B + \nu\alpha A_{-(N-q)})A_0^{-1} \quad (24)$$

is a matrix that describes the coupling and local dynamics of the virtual network and

$$W^{\text{in}} := \nu\alpha\gamma A_0(\text{Id} - \nu\alpha A_q)^{-1}W^{\text{mask}} \quad (25)$$

is the generalized input matrix.

Equation (23) is the main result of this section, it allows us to calculate directly some figures of merit in the following. We first use it to explain the drops in the memory capacity in figure 2 for resonant delays. One important aspect to note, is that the basic shape of equation (23) does not change with τ' . Rather, a changing of the clock cycle leads to a change of the evolution matrices A and W^{in} of the equivalent network. The obtained system (23) can be equivalently considered as a specific echo state network.

5 Direct calculation of memory capacity

One can find an estimation for the memory capacity of a reservoir computing system by solving the system numerically and let it perform the memory task. But there are also analytic methods for some cases. In this section we explain how to calculate analytically the memory capacity of the linear echo state network (23).

Memory capacity was originally defined by Jaeger in [10]. In the following, we use a slightly modified formulation. Let the elements $u(k)$ of the input sequence be independently $\mathcal{N}(0, 1)$ -distributed. Jaeger introduced the quantity MC_d which indicates how well the output $\hat{y}(k)$ of an ESN may approximate the input value $u(k-d)$ which was fed into the reservoir d time steps earlier. The memory capacity for a recall of d time steps in the past is defined by

$$\text{MC}_d := \max_{W^{\text{out}}} \left(1 - \frac{\text{E}[(W^{\text{out}}X(k+d) - u(k))^2]}{\text{var}(u(k))} \right), \quad (26)$$

where E denotes the expectation value and we require the initial state $X(0)$ of the reservoir to be stationary distributed in order to ensure that this definition is consistent, i.e. that the distribution of $X(k)$ does not depend on k . For the existence of the stationary distribution, we assume $\rho(A) < 1$. In such a case, the memory capacity (26) with stationary distributed $X(0)$ can be equivalently

written as

$$\begin{aligned} \text{MC}_d &:= \max_{W^{\text{out}}} \left(1 - \frac{\mathbb{E}[(W^{\text{out}} X(d) - u(0))^2]}{\text{var}(u(0))} \right) \\ &= 1 - \min_{W^{\text{out}}} \mathbb{E}[(W^{\text{out}} X(d) - u(0))^2]. \end{aligned} \quad (27)$$

Note that $u(0) \sim \mathcal{N}(0,1)$ means that we can drop the term $\text{var}(u(0))$ in (27).

The total memory capacity MC is defined as the sum of all d -step memory capacities

$$\text{MC} := \sum_{d=1}^{\infty} \text{MC}_d. \quad (28)$$

In the following we denote the optimal output weight vector for (27) by W_d^{out} . Let Σ be the covariance matrix of the stationary distribution of the reservoir. Jaeger [10] noted that, if Σ is invertible, one can apply the Wiener-Hopf equation [26] to find

$$W_d^{\text{out}} = (A^{d-1} W^{\text{in}})^T \Sigma^{-1}. \quad (29)$$

For details we refer to Appendix B. Using this optimal value W_d^{out} , the memory capacity (27) can be calculated as

$$\text{MC}_d = (A^{d-1} W^{\text{in}})^T \Sigma^{-1} A^{d-1} W^{\text{in}}, \quad (30)$$

where we have used the relations

$$\begin{aligned} \mathbb{E}[W_d^{\text{out}} X(d) u(0)] &= \text{cov}(W_d^{\text{out}} X(d), u(0)) \\ &= (A^{d-1} W^{\text{in}})^T \Sigma^{-1} A^{d-1} W^{\text{in}} \end{aligned} \quad (31)$$

and

$$\begin{aligned} \mathbb{E}[(W_d^{\text{out}} X(d))^2] &= \text{var}(W_d^{\text{out}} X(d)) \\ &= (A^{d-1} W^{\text{in}})^T \Sigma^{-1} A^{d-1} W^{\text{in}}. \end{aligned} \quad (32)$$

So once the covariance matrix of the reservoir X is invertible, one can directly calculate the memory capacity. The stationary distribution of system (23) with standard normal distributed input elements $u(k)$ is a multivariate normal distribution with mean zero and covariance matrix

$$\Sigma = \sum_{j=0}^{\infty} A^j W^{\text{in}} (W^{\text{in}})^T A^{jT}. \quad (33)$$

We refer to Appendix B for a derivation. However, this matrix is in general not invertible. In order to obtain an invertible covariance matrix, we need to perturb the stochastic process (23). We choose a small number $\sigma_\eta > 0$ and let

$\eta(k) \sim \mathcal{N}(0, \text{Id})$ be a sequence of independent multivariate normal distributed random variables. The stochastic process

$$X(k+1) = AX(k) + W^{\text{in}}u(k) + \sigma_\eta \eta(k), \quad (34)$$

has the stationary distribution $\mathcal{N}(0, \Sigma_\eta)$, where the covariance matrix given by

$$\Sigma_\eta = \sum_{j=0}^{\infty} A^j (W^{\text{in}}(W^{\text{in}})^{\text{T}} + \sigma_\eta \text{Id}) A^{j\text{T}} \quad (35)$$

is invertible.

6 Explanation for memory capacity gaps

Using the expressions (28) and (30) for the memory capacity obtained in section 5, we provide an explanation for the loss of the memory capacity when τ'/τ is close to rational numbers with small denominator. The explanation is based on the structure of the covariance matrix Σ_η given by equation (35) and the corresponding expression for the memory capacity, which we repeat here for convenience

$$\begin{aligned} \text{MC} &= \sum_{d=1}^{\infty} \text{MC}_d, \\ \text{MC}_d &= (A^{d-1}W^{\text{in}})^{\text{T}} \Sigma_\eta^{-1} A^{d-1}W^{\text{in}}, \end{aligned} \quad (36)$$

where

$$\begin{aligned} \Sigma_\eta &= \sum_{j=0}^{\infty} (\Pi_j + \sigma_\eta A^j A^{j\text{T}}), \\ \Pi_j &:= A^j W^{\text{in}} (W^{\text{in}})^{\text{T}} A^{j\text{T}}. \end{aligned} \quad (37)$$

Our further strategy is as follows:

- (i) Firstly, we remark that the norms of the individual terms in the sum (37) are converging to zero due to the convergence of the series. Hence, only the first finitely many terms play an important role. For instance, for our previously chosen parameters in figure 2, the terms with $j \gtrsim 30$ do not make a large contribution and can be neglected. In the following we denote the approximate number of significant terms by j_n .
- (ii) We show that the largest eigenvalue of the j -th term in (37) can be approximated by $\|A^j W^{\text{in}}\|^2$ with the corresponding eigenvector $A^j W^{\text{in}}$.
- (iii) We show that the memory capacity is high, i.e. $\text{MC}_d \approx 1$ for $d \leq j_n$, when the eigenvectors $A^j W^{\text{in}}$ corresponding to the first relevant terms in the sum (37) are orthogonal.

- (iv) Using our setup, we show numerically that the lower order resonances $\tau'/\tau = a/b$, where $a, b \in \mathbb{N}$ and b is small, lead to the alignment of the eigenvectors $A^j W^{\text{in}}$, and hence, to the loss of the memory capacity.
- (v) Finally we give an intuitive explanation of the obtained orthogonality conditions.

Remark (i) is obvious, so we start with showing (ii).

(ii) Estimating the largest eigenvalues and eigenvectors of the j -th term in (37) Consider at first the term with $j = 0$: $W^{\text{in}}(W^{\text{in}})^{\text{T}} + \sigma_\eta \text{Id}$. The largest eigenvalue of this matrix is $\|W^{\text{in}}\|_2^2 + \sigma_\eta$ and the corresponding eigenvector is W^{in} as can be easily checked by the direct calculation

$$[W^{\text{in}}(W^{\text{in}})^{\text{T}} + \sigma_\eta \text{Id}]W^{\text{in}} = (\|W^{\text{in}}\|_2^2 + \sigma_\eta)W^{\text{in}}. \quad (38)$$

For all other eigenvectors v , which are orthogonal to W^{in} due to the symmetry of the matrix, the corresponding eigenvalues are σ_η because

$$[W^{\text{in}}(W^{\text{in}})^{\text{T}} + \sigma_\eta \text{Id}]v = W^{\text{in}}\langle W^{\text{in}}, v \rangle + \sigma_\eta v = \sigma_\eta v. \quad (39)$$

These eigenvalues are by definition small, since σ_η is a small perturbation.

We can also find approximations of the eigenvectors and eigenvalues for the higher order terms $\Pi_j + \sigma_\eta A^j A^{j\text{T}}$, $j > 0$. Namely, for the unperturbed matrix Π_j , the largest eigenvalue is $\|A^j W^{\text{in}}\|^2$ and the corresponding eigenvector is $A^j W^{\text{in}}$ because

$$\begin{aligned} \Pi_j A^j W^{\text{in}} &= [A^j W^{\text{in}}(W^{\text{in}})^{\text{T}} A^{j\text{T}}] A^j W^{\text{in}} \\ &= A^j W^{\text{in}} \langle A^j W^{\text{in}}, A^j W^{\text{in}} \rangle \\ &= \|A^j W^{\text{in}}\|_2^2 A^j W^{\text{in}}. \end{aligned} \quad (40)$$

All other eigenvalues are zero. Since the largest eigenvalue of Π_j is geometrically and algebraically simple, it is continuous under the perturbation by $\sigma_\eta \text{Id}$. Hence, the largest eigenvalue and the eigenvector of $\Pi_j + \sigma_\eta A^j A^{j\text{T}}$ are approximated by $\|A^j W^{\text{in}}\|^2$ and $A^j W^{\text{in}}$ with an error of order σ_η . All other eigenvalues are correspondingly small of order σ_η .

(iii) The orthogonality of $A^j W^{\text{in}}$ leads to the high memory capacity Let j_n be the number of terms in (37) that are significant (see (i)), and let us assume that the eigenvectors $A^j W^{\text{in}}$, $j = 0, 1, \dots, j_n$ are close to be orthogonal, i.e.

$$|\langle A^j W^{\text{in}}, A^i W^{\text{in}} \rangle| \ll 1, \quad i, j = 0, 1, \dots, j_n, \quad j \neq i. \quad (41)$$

As we will see in (iv), such an assumption is indeed reasonable in our setup. More precisely, one could consider (41) as $|\langle A^j W^{\text{in}}, A^i W^{\text{in}} \rangle| < \varepsilon$ introducing another small parameter $\varepsilon \ll 1$.

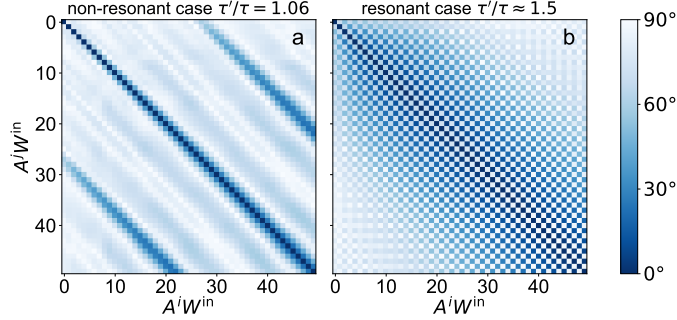


Figure 3: The angles between $A^j W^{\text{in}}$ and $A^i W^{\text{in}}$, $i, j = 1, \dots, 50$ are plotted in color, measuring, in particular, the orthogonality of the vectors $A^j W^{\text{in}}$ with different j . Panels (a) and (b) correspond to different ratios of τ'/τ : (a) $\tau'/\tau = 1.06$; (b) $\tau'/\tau = 1.52 \gtrsim 3/2$. In (b) the vectors $A^j W^{\text{in}}$ point into the same direction for $j, j+2, j+4$, etc., i.e. after two time steps the input values $u(k)$ overlap in the state space of X and the memory capacity drops. In contrast, in the case $\tau'/\tau = 1.06$ (a) it takes almost 30 time steps before the input overlaps with past inputs in the network state. This explains the high memory capacity in this case, which is illustrated in figure 2.

In case, when the orthogonality (41) holds, the largest eigenvalues of Σ_η and their corresponding eigenvectors can be approximated by $\|A^j W^{\text{in}}\|^2$ and $A^j W^{\text{in}}$, $j = 0, \dots, j_n$. Indeed

$$\begin{aligned} \Sigma_\eta A^j W^{\text{in}} &= \sum_{k=0}^{\infty} (\Pi_k A^j W^{\text{in}} + \sigma_\eta A^k A^{kT} A^j W^{\text{in}}) \\ &= \|A^j W^{\text{in}}\|_2^2 A^j W^{\text{in}} + \mathcal{O}(\sigma_\eta) + \mathcal{O}(\varepsilon). \end{aligned} \quad (42)$$

In this case, the memory capacity can be calculated as follows:

$$\begin{aligned} \text{MC}_d &= (A^{d-1} W^{\text{in}})^T \Sigma_\eta^{-1} A^{d-1} W^{\text{in}} \\ &= (A^{d-1} W^{\text{in}})^T \frac{1}{\|A^{d-1} W^{\text{in}}\|_2^2} A^{d-1} W^{\text{in}} + \mathcal{O}(\sigma_\eta) + \mathcal{O}(\varepsilon) \\ &= 1 + \mathcal{O}(\sigma_\eta) + \mathcal{O}(\varepsilon) \end{aligned} \quad (43)$$

for $d \leq j_n$. Hence, the orthogonality of the vectors $A^j W^{\text{in}}$ with $A^i W^{\text{in}}$, $i \neq j$ guarantees a high memory capacity. We will present an intuitive explanation for this shortly.

(iv) Resonances of τ' and τ lead to lower memory capacity The plots in figure 3 show $\langle A^j W^{\text{in}}, A^i W^{\text{in}} \rangle$ for different ratios τ'/τ . White to light blue off-diagonal squares indicate that assumption (41) is satisfied, i.e. orthogonal or almost orthogonal vectors. Dark blue indicates a strong parallelism of the

vectors. As can be seen in the top panel of figure 3, the assumption (41) holds indeed for ratios τ'/τ which yield a good memory performance. Conversely, it is strongly violated for critical ratios $\tau'/\tau \gtrsim a/b$ with small denominator b , e.g. the center panel of figure 3.

(v) Intuitive explanations There is an additional intuitive understanding of the above derived formulas. Recall that the original system of the reservoir of equation (9) combines the delay term $x(t - \tau)$ and the input $J(t)$ additively. The approximated network formula for an equivalent network translated this into the matrix A , which describes the free dynamics of the network, and the driving term defined by W^{in} . The state of the network is given by an N -dimensional system, and thus can at most hold N orthogonal dimensions [27]. Each summand of Σ_η can now be understood as an imprint of the driving term on the system after j time steps. For $j = 0$ the matrix $A^0 = \text{Id}$, and thus the imprint is given by W^{in} , i.e. the information of the current step is stored in the nodes as given by the weights of the effective input weight vector W^{in} . In the next step, the system will get an additional input, but also evolve according to its local dynamics A . Thus, after one time step, the imprint has transformed into AW^{in} , i.e. the summand for $j = 1$ and $\sigma_\eta \rightarrow 0$. Now in every step, the information that is currently present in the network will be ‘rotated’ in the phase space of the network according to A , while a new input will be projected onto the direction of W^{in} . This holds in general, so that the j th summand of Σ_η of equation (35) $A^j W^{\text{in}}$ describes the linear imprint of the input j steps in the past.

The orthogonality condition of equation (41) then is the same concept as demanding that new information from the inputs should not overwrite the already present information. If $A^r \approx s\text{Id}$ for some $s \in \mathbb{R}$, then the information that was stored from r steps in the past will be partially overwritten by the currently injected step and lost. Hence, ensuring that the orthogonality between $A^j W^{\text{in}}$ is fulfilled as much as possible will maximize the linear memory. For the case of resonant feedback, i.e. $\tau' = \tau$, this condition is not fulfilled. This is due to the fact, that A has a strong diagonal component for the resonant cases, i.e. virtual nodes are most strongly coupled to themselves. This is a simple consequence of the fact that for $\tau = \tau'$, virtual nodes return to the single real node at the same time that they are updated. Similarly, for higher resonant cases $b\tau' = a\tau$, A^b will in general have a strong diagonal part and thus the eigenvector $A^b W^{\text{in}}$ will not be orthogonal to $A^0 W^{\text{in}}$, and the information will be overwritten.

7 Discussion

In this paper we have shown a generalization of the frequently used time-delay reservoir computing for cases other than $\tau' = \tau$. We observed that a sudden increase in the computing error (NARMA-10 NRMSE) and a drop in the linear memory capacity (MC) can be seen for resonant cases of $b\tau' = a\tau$ with $a, b \in \mathbb{N}$, where b is small. We derived an equivalent network for the non-resonant cases

which extends the previously studied cases. Assuming a linear activation function $f(x) = \alpha x$, we can analytically solve the resulting implicit equations and obtain an expression for the total memory capacity MC. Here we find that the resulting memory capacity will be small for cases where τ and τ' are resonant because the information within the equivalent network will be overwritten by new inputs very quickly. Even though our analytics so far are only derived for the linear case, we expect these results to hold in general, as numerical investigations imply. We have also found that the observed effect is more pronounced in smaller networks and with stronger regularization.

Acknowledgements

S.Y. acknowledges the financial support by the Deutsche Forschungsgemeinschaft (DFG, German Research Foundation) - Project 411803875. A.R. and K.L. acknowledge support from the Deutsche Forschungsgemeinschaft in the framework of the CRC910. F.S. acknowledges financial support provided by the Deutsche Forschungsgemeinschaft through the IRTG 1740.

Appendix

A Derivation of equivalent networks

This section presents a detailed derivation of the ESN representation of TDRC systems. The derivation is structured as follows:

1. The delay system (9) is discretized such that the state of a virtual node $x(k\tau' + n\theta)$ depends on the state of its neighbor node $x(k\tau' + (n-1)\theta)$, the input $J_{k,n}$ and the state of a second node $x(k'\tau' + n'\theta)$ at the time $k' \leq k$. In order to do so, we approximate the integral of the continuous TDRC system on a small integration interval of length θ which covers the point $x(k'\tau' + n'\theta)$.
2. The formulas for n' and k' are derived.
3. The TDRC system can be written as a matrix equation. For this we use the same vectorization (10) of $x(t)$ as for the readout. An induction argument is employed to obtain the matrix equation.
4. It follows that the discretized TDRC system can be represented by an ESN if $\tau \leq \tau' - \theta$ and if the activation function f is linear.
5. For the sake of completeness, we formulate the equivalent ESN for the classical case $\tau' = \tau$, which was described in [12].

A.1 The delay reservoir system and discretization

Consider the delay-system (9), which we repeat here for convenience:

$$\dot{x}(t) = -x(t) + f[x(t - \tau) + \gamma J(t)], \quad (44)$$

where $\tau > 0$, $\gamma > 0$ and $f: \mathbb{R} \rightarrow \mathbb{R}$.

It follows that

$$e^{t-t_0}x(t) = x(t_0) + \int_{t_0}^t e^{s-t_0} f[x(s - \tau) + \gamma J(s)] ds \quad (45)$$

for $t \geq t_0$. Set $t_0 = k\tau' + (n-1)\theta$ and $t = k\tau' + n\theta$. Then

$$\begin{aligned} x(k\tau' + n\theta) &= e^{-\theta} x(k\tau' + (n-1)\theta) \\ &+ \int_0^\theta e^{s-\theta} f[x(k\tau' + (n-1)\theta + s - \tau) + \gamma J_{k,n}] ds, \end{aligned} \quad (46)$$

where $J_{k,n}$ is defined in (7). One option to discretize the system, is to approximate the function x by a step function with step length θ which is constant on the integration interval. One can find an appropriate step function by choosing $k'(k, n)$ and $n'(n)$ such that

$$k'\tau' + n'\theta \in (k\tau' + (n-1)\theta - \tau, k\tau' + n\theta - \tau] \quad (47)$$

and defining $x(t) \approx \tilde{x}(t) := x(k'\tau' + n'\theta)$ for $t \in (k\tau' + (n-1)\theta - \tau, k\tau' + n\theta - \tau]$. Then, one can replace x by \tilde{x} in the integrand in equation (46). This yields

$$\begin{aligned} &x(k\tau' + n\theta) \\ &\approx e^{-\theta} x(k\tau' + (n-1)\theta) \\ &+ \int_0^\theta e^{s-\theta} f[x(k'(k, n)\tau' + n'(n)\theta) + \gamma J_{k,n}] ds \\ &= e^{-\theta} x(k\tau' + (n-1)\theta) \\ &+ (1 - e^{-\theta}) f[x(k'(k, n)\tau' + n'(n)\theta) + \gamma J_{k,n}]. \end{aligned} \quad (48)$$

A.2 The choice of k' and n'

The floor and the ceiling function are denoted by $\lfloor \cdot \rfloor$ and $\lceil \cdot \rceil$, respectively. One can choose k' and n' in the following way:

First, let $m \in \mathbb{Z}$, $m \geq 1$ be the unique number such that $\tau \in ((m-1)\theta, m\theta]$, i.e. $m = \lceil \tau/\theta \rceil$. Then

$$k'\tau' + n'\theta = k\tau' + n\theta - m\theta \quad (49)$$

as illustrated in figure 4. Now, the choice of n' follows directly from the restriction $n' \in \{1, \dots, N\}$. It holds that

$$n'(n) = \begin{cases} (n-m) \bmod N, & \text{if } N \nmid (n-m), \\ N, & \text{if } N \mid (n-m). \end{cases} \quad (50)$$

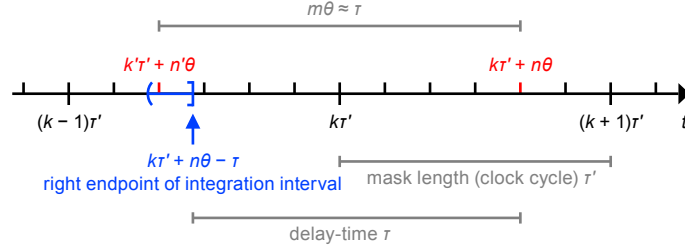


Figure 4: The time interval over which the function x is integrated in equation (46) is highlighted in blue. As stated in equation (47), the point $k'\tau' + n'\theta$ must be chosen such that it lies within this interval. In equation (48) the value of x on the integration interval is approximated by the value of $x(k'\tau' + n'\theta)$. If the endpoints of the interval are grid points, $k'\tau' + n'\theta$ is chosen to be the right endpoint.

From this result follows that

$$\begin{aligned}
 (n-m)\theta &= n'\theta + N\theta \cdot \begin{cases} \lfloor \frac{n-m}{N} \rfloor, & \text{if } N \nmid (n-m), \\ \frac{n-m}{N} - 1, & \text{if } N \mid (n-m), \end{cases} \\
 &= n'\theta + \left(\left\lfloor \frac{n-m}{N} \right\rfloor - 1 \right) \tau'.
 \end{aligned} \tag{51}$$

Hence, equation (49) implies

$$k'(k, n) = k + \left\lfloor \frac{n-m}{N} \right\rfloor - 1. \tag{52}$$

Note that one has $k' = k$ as long as $n-m \in \{1, n-1\}$. If $n-m \in \{-N+1, \dots, 0\}$, then $k' = k-1$. For $n-m \in \{-2N+1, \dots, -N\}$ holds $k' = k-2$, etc.

A.3 Vectorization of the state space and a matrix equation for the discretized system

Define

$$X(k) := \begin{pmatrix} X_1(k) \\ \vdots \\ X_N(k) \end{pmatrix} := \begin{pmatrix} x((k-1)\tau' + \theta) \\ x((k-1)\tau' + 2\theta) \\ \vdots \\ x((k-1)\tau' + N\theta) \end{pmatrix} \tag{53}$$

and $\tilde{f} \equiv (1 - e^{-\theta})f$. From (48) follows

$$\begin{aligned}
 X_1(k+1) &= x(k\tau' + \theta) \\
 &= e^{-\theta} x(k\tau') + \tilde{f}[x(k'(k, 1)\tau' + n'(1)\theta) + \gamma J_{k,1}] \\
 &= e^{-\theta} X_N(k) + \tilde{f}[X_{n'(1)}(k'(k, 1) + 1) + \gamma J_{k,1}]
 \end{aligned} \tag{54}$$

and induction yields

$$\begin{aligned}
& X_n(k+1) \\
&= e^{-n\theta} X_N(k) \\
&\quad + e^{-(n-1)\theta} \tilde{f}[X_{n'(1)}(k'(k,1)+1) + \gamma J_{k,1}] \\
&\quad + e^{-(n-2)\theta} \tilde{f}[X_{n'(2)}(k'(k,2)+1) + \gamma J_{k,2}] \\
&\quad \vdots \\
&\quad + e^{-\theta} \tilde{f}[X_{n'(n-1)}(k'(k,n-1)+1) + \gamma J_{k,n-1}] \\
&\quad + \tilde{f}[X_{n'(n)}(k'(k,n)+1) + \gamma J_{k,n}]
\end{aligned} \tag{55}$$

for $n \in \{2, \dots, N\}$.

These equations can be rewritten as a matrix equation. Let

$$A_0 := \begin{pmatrix} 1 & 0 & \dots & 0 \\ e^{-\theta} & 1 & \ddots & \vdots \\ \vdots & \ddots & \ddots & 0 \\ e^{-(N-1)\theta} & \dots & e^{-\theta} & 1 \end{pmatrix} \tag{56}$$

and

$$\tilde{F} \begin{pmatrix} x_1 \\ \vdots \\ x_N \end{pmatrix} := \begin{pmatrix} \tilde{f}(x_1) \\ \vdots \\ \tilde{f}(x_N) \end{pmatrix}. \tag{57}$$

Then

$$\begin{aligned}
X(k+1) &= A_0 \tilde{F} \begin{pmatrix} X_{n'(1)}(k'(k,1)+1) + \gamma J_{k,1} \\ \vdots \\ X_{n'(N)}(k'(k,N)+1) + \gamma J_{k,N} \end{pmatrix} \\
&\quad + \begin{pmatrix} e^{-\theta} X_N(k) \\ \vdots \\ e^{-N\theta} X_N(k) \end{pmatrix}
\end{aligned} \tag{58}$$

Let $\ell := \lfloor m/N \rfloor$ and $q := m \bmod N$, as defined in (16), i.e $m = \ell N + q$. By plugging this into equation (50) and noting that $1 \leq n \leq N$ and $0 \leq q \leq N-1$, one obtains

$$n'(n) = \begin{cases} n - q + N, & \text{for } n \leq q, \\ n - q, & \text{for } n > q, \end{cases} \tag{59}$$

and by replacing m by $\ell N + q$ equation (52) follows

$$k'(k, n) = \begin{cases} k - \ell, & n > q, \\ k - \ell - 1, & n \leq q. \end{cases} \tag{60}$$

Hence, the vector $(X_{n'(n)}(k'(k, n) + 1))_{n=1, \dots, N}$ can be written as follows:

$$\begin{pmatrix} X_{n'(1)}(k'(k, 1) + 1) \\ \vdots \\ X_{n'(N)}(k'(k, N) + 1) \end{pmatrix} = \begin{pmatrix} 0 \\ \vdots \\ 0 \\ X_1(k + 1 - \ell) \\ \vdots \\ X_{N-q}(k + 1 - \ell) \end{pmatrix} + \begin{pmatrix} X_{N-q+1}(k - \ell) \\ \vdots \\ X_N(k - \ell) \\ 0 \\ \vdots \\ 0 \end{pmatrix}. \quad (61)$$

Thus, the map (58) can be written as

$$\begin{aligned} X(k + 1) &:= A_0 \tilde{F}[M_q X(k + 1 - \ell) \\ &+ M_{-(N-q)} X(k - \ell) + \gamma J_k] + A_0 \begin{pmatrix} e^{-\theta} X_N(k) \\ 0 \\ \vdots \\ 0 \end{pmatrix}, \end{aligned} \quad (62)$$

where the matrices $M_q = (\delta_{i, j+q})_{1 \leq i, j \leq N}$ and $M_{-(N-q)} = (\delta_{i, j-(N-q)})_{1 \leq i, j \leq N}$ are shift matrices.

The matrix A_0 is invertible and can be used to transform the system. Let $\tilde{X} := A_0^{-1} X$. Then

$$\begin{aligned} \tilde{X}(k + 1) &= B \tilde{X}(k) + \tilde{F}[A_q \tilde{X}(k + 1 - \ell) \\ &+ A_{-(N-q)} \tilde{X}(k - \ell) + \gamma J_k], \end{aligned} \quad (63)$$

where the matrix

$$A_q = M_q A_0 = \begin{pmatrix} 0 & \cdots & \cdots & \cdots & \cdots & \cdots & 0 \\ \vdots & & & & & & \vdots \\ 0 & & & & & & \vdots \\ 1 & 0 & & & & & \vdots \\ e^{-\theta} & 1 & \ddots & & & & \vdots \\ \vdots & \ddots & \ddots & 0 & & & \vdots \\ e^{-(N-1-q)\theta} & \cdots & e^{-\theta} & 1 & 0 & \cdots & 0 \end{pmatrix} \quad (64)$$

is obtained by a q rows downwards shift of A_0 and the matrix

$$A_{-(N-q)} = M_{-(N-q)}A_0 = \begin{pmatrix} e^{-(N-q)\theta} & \dots & e^{-2\theta} & e^{-\theta} & 1 & 0 & \dots & 0 \\ \vdots & & & \ddots & \ddots & \ddots & \ddots & \vdots \\ \vdots & & & & \ddots & \ddots & \ddots & 0 \\ e^{-(N-1)\theta} & \dots & \dots & \dots & \dots & e^{-2\theta} & e^{-\theta} & 1 \\ 0 & \dots & \dots & \dots & \dots & 0 & 0 & 0 \\ \vdots & & & & & & & \vdots \\ 0 & \dots & \dots & \dots & \dots & \dots & \dots & 0 \end{pmatrix} \quad (65)$$

is obtained by an $N - q$ rows upwards shift of A_0 and

$$B = \begin{pmatrix} e^{-N\theta} & \dots & e^{-\theta} \\ 0 & \dots & 0 \\ \vdots & & \vdots \\ 0 & \dots & 0 \end{pmatrix}. \quad (66)$$

The equation (66) for matrix B follows from equation (62). It must hold that

$$\begin{pmatrix} e^{-\theta}X_N(k) \\ 0 \\ \vdots \\ 0 \end{pmatrix} = B\tilde{X}(k) = BA_0^{-1}X(k). \quad (67)$$

Hence,

$$B = \begin{pmatrix} 0 & \dots & 0 & e^{-\theta} \\ 0 & \dots & \dots & 0 \\ \vdots & & & \vdots \\ 0 & \dots & \dots & 0 \end{pmatrix} A_0. \quad (68)$$

A.4 An ESN representation of TDRC systems with suitable parameters

If $\tau \leq \tau' - \theta$, then $\ell = 0$. This follows from the definitions $\ell := \lfloor m/N \rfloor$ and $m = \lceil \tau/\theta \rceil$. Equation (63) is in this case an implicit map:

$$\begin{aligned} \tilde{X}(k+1) &= B\tilde{X}(k) \\ &+ \tilde{F}[A_q\tilde{X}(k+1) + A_{-(N-q)}\tilde{X}(k) + \gamma J_k]. \end{aligned} \quad (69)$$

However, for a linear activation function $f(x) = \alpha x$, where α is a scalar, holds $\tilde{f}(x) = (1 - e^{-\theta})\alpha x$ and hence one obtains the explicit linear map

$$\begin{aligned} \tilde{X}(k+1) &= (\text{Id} - \nu\alpha A_q)^{-1}(B + \nu\alpha A_{-(N-q)})\tilde{X}(k) \\ &+ \nu\alpha\gamma(\text{Id} - \nu\alpha A_q)^{-1}J_k, \end{aligned} \quad (70)$$

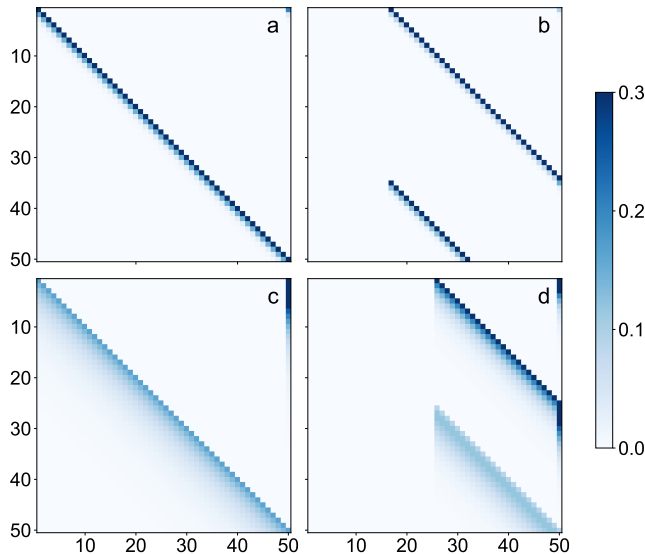


Figure 5: Plot of the network matrix A , given by (72) resp. (77), for $N = 50$ and (a) $\tau = 80$, $\tau' = 80$, (b) $\tau = 80$, $\tau' = 120$, (c) $\tau = 10$, $\tau' = 10$, (d) $\tau = 10$, $\tau' = 20$. The connection weights are truncated at 0.3. The panels (a) and (c) show matrices for the classical case. (See subsection A.5.) The panels (b) and (d) show matrices for the case $\tau \leq \tau' - \theta$ (subsection A.4). The strongest connection weights lie on diagonal lines which are shifted as the ratio of τ' and τ changes. The weights below these lines scale with the factor $e^{-n\theta}$, where n is the distance to the line. Since $\theta = \tau'/N$, the (off-diagonal) weights are larger in panels (c) and (d), where τ' is smaller.

where $\nu := 1 - e^{-\theta}$. Since $\tilde{X} = A_0^{-1}X$ and $J_k = W^{\text{mask}}u_k$, one can write this map in the original coordinates and in terms of the original input sequence

$$X(k+1) = AX(k) + Wu(k), \quad (71)$$

where

$$A := A_0(\text{Id} - \nu\alpha A_q)^{-1}(B + \nu\alpha A_{-(N-q)})A_0^{-1} \quad (72)$$

and

$$W^{\text{in}} := \nu\alpha\gamma A_0(\text{Id} - \nu\alpha A_q)^{-1}W^{\text{mask}}. \quad (73)$$

The network matrix A is plotted in figure 5 for different parameters.

A.5 The ESN representation of classical TDRC systems

The article [12] contains a description of an equivalent echo state network for TDRC systems with $\tau' = \tau$. This description is consistent with the case $\tau \in$

$(\tau' - \theta, \tau']$ in the framework of our discretization. In this case,

$$m = N, \quad \ell = 1, \quad q = 0, \quad (74)$$

and therefore, $A_q = A_0$ and $A_{-(N-q)}$ is the zero matrix. Thus, equation (63) simplifies to

$$\tilde{X}(k+1) = B\tilde{X}(k) + \tilde{F}[A_0\tilde{X}(k) + \gamma J_k]. \quad (75)$$

For a linear activation function $f(x) = \alpha x$, the equivalent network written in the original coordinates is

$$X(k+1) = AX(k) + Wu(k), \quad (76)$$

where

$$A := A_0BA_0^{-1} + \nu\alpha A_0 \quad (77)$$

and

$$W^{\text{in}} := \nu\alpha\gamma A_0 W^{\text{mask}}. \quad (78)$$

B Derivation of the memory capacity formula

We consider the linear echo state network

$$X(k+1) = AX(k) + W^{\text{in}}u(k), \quad (79)$$

where the input elements $u(k)$ are independently $\mathcal{N}(0, 1)$ -distributed. In section 5 we defined

$$\text{MC}_d = \max_{W^{\text{out}}} (1 - \mathbb{E}[(W^{\text{out}}X(k+d) - u(k))^2]) \quad (80)$$

and we claimed that

$$W_d^{\text{out}} = (A^{d-1}W^{\text{in}})^T \Sigma^{-1} \quad (81)$$

is the optimal argument for (80). In the following we show that W_d^{out} is indeed the optimal argument for (80).

In order to maximize (80), we need to minimize the mean square error

$$\begin{aligned} \text{MSE} &= \mathbb{E}[(W^{\text{out}}X(k+d) - u(k))^2] \\ &= \mathbb{E}[(W^{\text{out}}X(k+d))^2] + \mathbb{E}[u(k)^2] \\ &\quad - 2\mathbb{E}[W^{\text{out}}X(k+d)u(k)]. \end{aligned} \quad (82)$$

We know that $X(k) \sim \mathcal{N}(0, \Sigma)$ and hence

$$W^{\text{out}}X(k) \sim \mathcal{N}(0, W^{\text{out}}\Sigma(W^{\text{out}})^T). \quad (83)$$

Note that $W^{\text{out}}\Sigma(W^{\text{out}})^{\text{T}}$ is a scalar because W^{out} is a row vector. Since the mean of $W^{\text{out}}X(k+d)$ is zero and $u(k) \sim \mathcal{N}(0, 1)$, we have

$$\begin{aligned} \text{E}[(W^{\text{out}}X(k+d))^2] &= \text{var}(W^{\text{out}}X(k+d)) \\ &= W^{\text{out}}\Sigma(W^{\text{out}})^{\text{T}}, \end{aligned} \quad (84)$$

$$\text{E}[u(k)^2] = 1, \quad (85)$$

$$\text{E}[W^{\text{out}}X(k+d)u(k)] = \text{cov}(u(k), W^{\text{out}}X(k+d)). \quad (86)$$

Moreover,

$$\begin{aligned} &W^{\text{out}}X(k+d) \\ &= W^{\text{out}} \left(A^d X(k) + \sum_{j=0}^{d-1} A^j W^{\text{in}} u(k+d-1-j) \right) \end{aligned} \quad (87)$$

and $u(k)$ is independent of $X(k)$. Therefore,

$$\begin{aligned} &\text{cov}(u(k), W^{\text{out}}X(k+d)) \\ &= \text{cov}(u(k), W^{\text{out}}A^{d-1}W^{\text{in}}u(k)) \\ &= W^{\text{out}}A^{d-1}W^{\text{in}}. \end{aligned} \quad (88)$$

Thus, we obtain

$$\text{MSE} = W^{\text{out}}\Sigma(W^{\text{out}})^{\text{T}} + 1 - 2W^{\text{out}}A^{d-1}W^{\text{in}}. \quad (89)$$

Since the mean square error is quadratic in the argument $W^{\text{out}} = (w_1^{\text{out}}, \dots, w_N^{\text{out}})$, it has exactly one local minimum, which is the global minimum. A row vector W_d^{out} is the minimum argument if and only if

$$\frac{\partial}{\partial w_n^{\text{out}}} \text{MSE}(W_d^{\text{out}}) = 0, \quad n = 1, \dots, N. \quad (90)$$

For a quadratic form

$$Q(v) = v^{\text{T}}Mv, \quad (91)$$

where $v \in \mathbb{R}^N$ and M is a symmetric matrix, the vector of the partial derivatives is given by

$$\frac{\partial Q(v)}{\partial v} = 2v^{\text{T}}M. \quad (92)$$

Therefore,

$$\frac{\partial \text{MSE}}{\partial W^{\text{out}}} = 2W^{\text{out}}\Sigma - 2(A^{d-1}W^{\text{in}})^{\text{T}} \quad (93)$$

and hence

$$W_d^{\text{out}}\Sigma = (A^{d-1}W^{\text{in}})^{\text{T}}. \quad (94)$$

This formula is called Wiener-Hopf equation [26]. It follows that

$$W_d^{\text{out}} = (A^{d-1}W^{\text{in}})^{\text{T}}\Sigma^{-1}. \quad (95)$$

C The NARMA-10 benchmark

The 10th-order nonlinear autoregressive moving average (NARMA-10) task was introduced in [25] to evaluate the performance of machine learning methods on time series estimation. The NARMA-10 sequence $(y(k))_{k \geq 0}$ is defined as follows: for an input sequence with independently $\mathcal{U}(0, 0.5)$ -distributed elements $u(k)$, let

$$y(0) = y(1) = \dots = y(9) = 0 \quad (96)$$

and

$$y(k+1) = 0.3y(k) + 0.05y(k) \left(\sum_{j=0}^9 y(k-j) \right) + 1.5u(k-9)u(k) + 0.1 \quad (97)$$

for $k \geq 9$.

In order to evaluate the performance of a reservoir computer, we choose sufficiently large numbers $k_0, K \in \mathbb{N}$ and we compare the output values $\hat{y}(k_0+1), \dots, \hat{y}(k_0+K)$ to the desired target values $y(k_0+1), \dots, y(k_0+K)$ by the normalized root mean square error

$$\text{NRMSE} = \left(\frac{1}{K} \sum_{k=k_0+1}^{k_0+K} \frac{(\hat{y}(k) - y(k))^2}{\text{var}(y)} \right)^{\frac{1}{2}}. \quad (98)$$

References

- [1] Herbert Jaeger. The “echo state” approach to analysing and training recurrent neural networks. *Ger. Natl. Res. Cent. Inf. Technol. GMD Tech. Rep.*, 148, 2001.
- [2] Wolfgang Maass, Thomas Natschläger, and Henry Markam. Real-time computing without stable states: A new framework for neural computation based on perturbations. *Neural Comput.*, 14(11):2531–2560, 2002.
- [3] Guy Van der Sande, Daniel Brunner, and M. C. Soriano. Advances in photonic reservoir computing. *Nanophotonics*, 6(3):561, May 2017.
- [4] Daniel Brunner, Bogdan Penkovsky, Bicky A. Marquez, M. Jacquot, Ingo Fischer, and Laurent Larger. Tutorial: Photonic neural networks in delay systems. *J. Appl. Phys.*, 124(15):152004, 2018.
- [5] Herbert Jaeger and Harald Haas. Harnessing Nonlinearity: Predicting Chaotic Systems and Saving Energy in Wireless Communication. *Science (80-.)*, 304(5667):78–80, apr 2004.

- [6] D. Verstraeten, B. Schrauwen, D. Stroobandt, and J. Van Campenhout. Isolated word recognition with the Liquid State Machine: a case study. *Inf. Process. Lett.*, 95(6):521–528, sep 2005.
- [7] D. Verstraeten, B. Schrauwen, and D. Stroobandt. Reservoir-based techniques for speech recognition. In *2006 IEEE Int. Jt. Conf. Neural Netw. Proc.*, pages 1050–1053. IEEE, 2006.
- [8] A. Argyris, J. Bueno, and I. Fischer. Photonic machine learning implementation for signal recovery in optical communications. *Sci. Rep.*, 8(8487):1–13, May 2018.
- [9] J Pathak, B Hunt, M Girvan, Z Lu, and E Ott. Model-Free Prediction of Large Spatiotemporally Chaotic Systems from Data: A Reservoir Computing Approach. *Phys. Rev. Lett.*, 120(2):24102, 2018.
- [10] Herbert Jaeger. Short Term Memory in Echo State Networks. *Ger. Natl. Res. Cent. Inf. Technol. GMD Tech. Rep.*, 152, 2002.
- [11] Thomas Lymburn, Alexander Khor, Thomas Stemler, Débora C. Corrêa, Michael Small, and Thomas Jüngling. Consistency in echo-state networks. *Chaos*, 29, 2019.
- [12] L Appeltant, M.C. Soriano, G Van der Sande, J Danckaert, S Massar, J Dambre, B Schrauwen, C.R. Mirasso, and I Fischer. Information processing using a single dynamical node as complex system. *Nat. Commun.*, 2(1):468, sep 2011.
- [13] A Röhm and K Lüdge. Multiplexed networks: reservoir computing with virtual and real nodes. *J. Phys. Commun.*, 2:85007, 2018.
- [14] Thomas Erneux. *Applied Delay Differential Equations*, volume 3 of *Surveys and Tutorials in the Applied Mathematical Sciences*. Springer, 2009.
- [15] Thomas Erneux, Julien Javaloyes, Matthias Wolfrum, and Serhiy Yanchuk. Introduction to Focus Issue: Time-delay dynamics. *Chaos An Interdiscip. J. Nonlinear Sci.*, 27(11):114201, nov 2017.
- [16] Serhiy Yanchuk and Giovanni Giacomelli. Spatio-temporal phenomena in complex systems with time delays. *J. Phys. A Math. Theor.*, 50(10):103001, mar 2017.
- [17] Daniel Brunner, Miguel C Soriano, Claudio R Mirasso, and Ingo Fischer. Parallel photonic information processing at gigabyte per second data rates using transient states. *Nat. Commun.*, 2, 2011.
- [18] L Larger, M C Soriano, D Brunner, L Appeltant, J M Gutierrez, L Pesquera, C R Mirasso, and I Fischer. Photonic information processing beyond Turing: an optoelectronic implementation of reservoir computing. *Opt. Express*, 20(3):3241–3249, jan 2012.

- [19] Yoma Kuriki, Joma Nakayama, Kosuke Takano, and Atsushi Uchida. Impact of input mask signals on delay-based photonic reservoir computing with semiconductor lasers. *Optics Express*, 26, 2018.
- [20] Nikolai F. Rulkov, Mikhail M. Sushchik, Lev S. Tsimring, and Henry D. I. Abarbanel. Generalized synchronization of chaos in directionally coupled chaotic systems. *Phys. Rev. E*, 51:980–994, Feb 1995.
- [21] Arkady Pikovsky, Michael Rosenblum, and Jürgen Kurths. *Synchronization: A universal concept in nonlinear science*. Cambridge University Press, 2001.
- [22] Johannes Schumacher, Hazem Toutounji, and Gordon Pipa. An analytical approach to single node delay-coupled reservoir computing. January 2013.
- [23] J Schumacher, H Toutounji, and G Pipa. An Analytical Approach to Single Node Delay-Coupled Reservoir Computing. Conference: 23rd International Conference on Artificial Neural Networks, 2013.
- [24] Y Paquot, F Duport, A Smerieri, J Dambre, B Schrauwen, M Haelterman, and S Massar. Optoelectronic Reservoir Computing. *Sci. Rep.*, 2(287), 2012.
- [25] Amir F Atiya and Alexander G Parlos. New Results on Recurrent Network Training: Unifying the Algorithms and Accelerating Convergence. *IEEE Trans. Neural Networks*, 11(3), 2000.
- [26] Simon Haykin. *Adaptive filter theory*. Prentice Hall, 3 edition, 1995.
- [27] J Dambre, D Verstraeten, B Schrauwen, and S Massar. Information processing capacity of dynamical systems. *Sci. Rep.*, 2:514, 2012.